*Proteins: Structure, Function, and Bioinformatics*

WILEY

PROTEINS

STRUCTURE NOTE

# Cryo-EM Structure of Human Hyaluronidase PH-20

Seong-Bin Im[1] | Hyung Nam Song[2] | Tae-Kyeong Jeong[1] | Nayun Kim[1] | Kyuwan Kim[2] | Soon-Jae Park[2] | Byung-Ha Oh[1,3]

[1]Department of Biological Sciences, KAIST Institute for the Biocentury, Korea Advanced Institute of Science and Technology, Daejeon, Republic of Korea | [2]Alteogen, Daejeon, Republic of Korea | [3]Graduate Program of Engineering Biology, Korea Advanced Institute of Science and Technology, Daejeon, Republic of Korea

**Correspondence:** Byung-Ha Oh (bhoh@kaist.ac.kr)

**Received:** 14 October 2024 | **Revised:** 8 December 2024 | **Accepted:** 16 December 2024

**Funding:** This work was supported by National Research Foundation of Korea Grant no (2023R1A2C3007329, NRF-2021M3A9G8025599, RS-2024-00508861, and RS-2024-00467046) and Alteogen Inc.

**Keywords:** Cryo-EM structure | Hyaluronidase | PH-20

## ABSTRACT

PH-20 is a specific type of hyaluronidase that plays a critical role in the fertilization process by facilitating the initial binding of sperm to the glycoprotein layer surrounding the oocyte and subsequently breaking down hyaluronic acid polymers in the cumulus cell layer. PH-20 contains an epidermal growth factor (EGF)-like domain, which may be involved in the recognition of the glycoprotein layer in addition to the catalytic domain. Herein, we report the structure of human PH-20 determined by cryogenic electron microscopy. Comparative analyses of the PH-20 structure with two other available hyaluronidase structures reveal a general similarity in the central catalytic domains, including the conservation of catalytically essential residues at the equivalent spatial positions. However, unique difference is found in the EGF-like domain, characterized by a longer sequence that is likely to form a flexibly anchored β-hairpin containing a disulfide bond.

## 1 | Introduction

Hyaluronic acid (HA) or hyaluronan is a long linear polymer composed of more than 2000 repeating disaccharide units of N-acetyl-D-glucosamine (GlcNAc) and D-glucuronic acid (GlcUA). This non-sulfated glycosaminoglycan is a major polysaccharide component of the extracellular matrix (ECM) of vertebrate tissues [1–4], and is especially abundant in loose connective tissues, such as skin and skeletal tissues [5]. Owing to a high degree of polymerization and an extremely hygroscopic property, HA forms a viscoelastic meshwork in the ECM [6], and plays diverse physiological roles, including lubrication, water homeostasis, and macromolecular filtering. As an ECM component, HA also plays important roles in cell proliferation, adhesion, and migration [5, 7] by interacting with HA-binding proteins (called hyaladherin) and cell-surface receptors, such as CD44 or RHAMM [8–10]. The activities of HA depend on its size; while HA with high molecular weight (> 1 MDa) is anti-inflammatory and anti-angiogenic, HA with low molecular weight have opposing effects on inflammation and angiogenesis [11]. Interestingly, the naked mole rat accumulates high-molecular-weight HA, and it is associated with longevity and cancer resistance [12, 13].

Mammalian hyaluronidases (HYALs) hydrolyze HA by cleaving the β (1 → 4) glycosidic bond between GlcNAc and GlcUA of hyaluronan. The human genome encodes five sequence homologues of this enzyme: HYAL-1, -2, -3, -4, and PH-20 (also known as SPAM1 for sperm adhesion molecule 1). Human HYAL-1 is a lysosomal enzyme responsible for the hydrolysis of intracellular HA. The protein exhibits a narrow range of optimum pH (3–4.5) for the catalytic activity, in consistency with the low lysosomal pH [14]. Human HYAL-2 is another lysosomal hyaluronidase and specifically hydrolyzes high molecular weight HA [2, 15]. By glycosylphosphatidylinositol (GPI)-anchoring on the plasma membranes, HYAL-2 is known to locate on cell surface as well, where it displays hyaluronidase activity in a CD44-dependent

© 2024 Wiley Periodicals LLC.



Petitioner Merck, Ex. 1126, p. 1067
Merck Sharp & Dohme LLC v. Halozyme Inc.
PGR2025-00003

manner [16] and serves as a receptor for the oncogenic Jaagsiekte sheep retrovirus [17, 18]. HYAL-3 is expressed in mammalian testis and bone marrow [15], and exhibits intracellular localization [19]. Human HYAL-3 does not appear to possess a hyaluronidase activity [16, 20, 21], and its functional role remains obscure. HYAL-4 is not a hyaluronidase but a chondroitinase specific for chondroitin sulfate, a sulfated glycosaminoglycan. It preferentially cleaves the galactosaminidic linkage in the trisulfated tetra-saccharide sequence [21, 22].

PH-20 is the sperm hyaluronidase conserved among mammals [23]. PH-20 is a GPI-anchored and located on both the sperm plasma membrane and acrosomal membrane. It is involved in penetration of sperm through the viscous cumulus mass surrounding the zona pellucida layer of the egg by hydrolyzing HA in the intercellular matrix embedding the cumulus cells [23, 24]. In contrast with HYAL-1, PH-20 exhibits a bimodal activity profile, with mildly acidic and neutral pH optima [14, 24, 25], which appears adequate for hydrolyzing HA in the cumulus mass of the egg.

Clinically, animal-derived sperm hyaluronidases or recombinant PH-20 have been used to increase dispersion and adsorption of co-administered therapeutic drugs, including monoclonal antibodies [26–30]. In addition, hyaluronidases are currently used for reducing tissue damage resulting from extravasation of a drug and as an essential drug for the management of complications or unsatisfactory results associated with the aesthetic injection of HA-based fillers [27, 31]. Moreover, a number of clinical trials of half-life extended PEGylated PH-20 have been made in HA-high pancreatic, lung, gastric, and HER2-negative breast cancers to enhance the delivery of circulating anticancer drugs to tumor cells by HA breakdown within the tumor [32, 33].

To date, the empirical three-dimensional information of this enzyme has been unavailable, although crystal structures of human HYAL-1 [34] and bee venom hyaluronidase (bvHyal) [35] have been determined. Herein, we report the cryogenic electron microscopy (cryo-EM) structure of human PH-20 at 3.1 Å resolution, providing a foundation for studying the functional and the catalytic property of PH-20.

## 2 | Results and Discussion

### 2.1 | Structure Determination

Human PH-20 (isoform 1; Uniprot ID: P38567-1) consists of 509 amino acids, with a predicted signal peptide (residues 1–35), propeptide (residues 36–41), a central glycohydrolase domain (residues 42–369), an epidermal growth factor (EGF)-like domain for zona pellucida recognition (residues 375–479), GPI-anchoring region (residues 484–509) in which Ser490 is the likely site for GPI-transamidation site [36, 37]. The C-terminal segment (residues 436–509), including a C-terminal portion of the EFG-like domain is completely disordered according to AlphaFold2 (AF2) prediction [38].

Initially, a truncated PH-20 construct comprising residues Leu36-Tyr482, excluding the GPI-anchoring region, was produced using Chinese hamster ovary (CHO) cells and subjected to crystallization trials. No crystals were obtained, likely due to the disordered nature of the C-terminal segment. Subsequently, another truncated construct, composed of residues Asn37-Phe468, herein is referred to as PH-20, was produced and crystallized. Albeit crystallized, this construct did not yield diffraction quality crystals, despite extensive crystallization screening. An antibody against PH-20, named 79C11, was discovered and its Fab (antigen-binding fragment) (79C11Fab) was employed as a crystallization chaperon, but failed to improve the crystal quality. We then resorted to cryo-EM to solve the three-dimensional structure of PH-20 bound to 79C11Fab (PH-20-79C11Fab). The cryo-EM data collection, processing, and refinement statistics are given in Table 1.

### 2.2 | Overall Structure

PH-20 adopts a $(\beta/\alpha)_8$-barrel fold, which is the most common fold among protein catalysts [40]. Unlike canonical $(\beta/\alpha)_8$-barrel structures characterized by eight parallel β-strands that interact sequentially and circularly to form a barrel-like shape, the barrel in PH-20 is distorted, exhibiting no main chain–main chain interaction between β2 (residues 74–78) and β3 (residues 87–91). In addition, the segment between β2 and β3 does not adopt an α-helix but a loop conformation. This open β-barrel is surrounded by α-helices with different lengths plus long segments connecting the alternating α-helix and β-strand, which dominates the overall shape of the protein molecule. The C-terminal segment following β8 (residues 335–339) is longest (~80 residues), comprising an EGF-like domain, to which 79C11Fab is bound. Overall, PH-20 has a deep and wide active site which appears suitable for binding and processing the long polymeric substrates (Figure 1).

### 2.3 | Structural Comparison

The crystal structures of human HYAL-1 and the full-length matured form of bvHyal have been reported [34, 35]. The molecular weight of the three hyaluronidase increases in the order of bvHyal, HYAL-1, and PH-20 (Figure 2A). BvHyal consists only of a catalytic domain. HYAL-1 has an additional EGF-like domain, and PH-20 contains an EGF-like domain and a C-terminal ~50-residue extension (Figure 2A). Notably, the EGF-like domain of PH-20 is extended compared with that of HYAL-1. However, the electron density for the extended segment (Cys443-Phe468) is not visible, and 79C11Fab binds to the visible portion of the EGF-like domain (Figure 2B). Interestingly, an AlphaFold3 (AF3) [41] predicted structure of PH-20-79C11Fab showed that 79C11Fab binds to a different surface, and the disordered segment forms a β-hairpin that forms a four-stranded β-sheet together with the preceding β-hairpin (Figure 2B). The confidence scores (pLDDT) of Cys443-Phe468 segment were 78–97 for backbone atoms. These observations support that the Cys443-Phe468 segment interacts weakly with the rest of PH-20, such that 79C11 antibody could have been discovered which displaces this segment. According to the AF3 prediction, the EGF-like domain of PH-20 has one more disulfide bond (Cys458-Cys464) in addition to the three disulfide bonds commonly found in other EGF-like domains including that of HYAL-1 (Figure S1). While the presence of the three disulfide bonds is a hallmark



Petitioner Merck, Ex. 1126, p. 1068
Merck Sharp & Dohme LLC v. Halozyme Inc.
PGR2025-00003

**TABLE 1** | Cryo-EM data collection, processing, and refinement statistics.

| | PH-20-79C11Fab |
|---|---|
| Data collection and processing | |
| Microscope | Titan Krios |
| Magnification | x130,000 |
| Voltage (kV) | 300 |
| Detector | Gatan K3 |
| Electron exposure (e−/Å2) | 69 |
| Defocus range (μm) | −0.8 to −2.3 |
| Pixel size (Å) | 0.664 |
| No. of frames | 48 |
| Movies | 20 709 |
| No. of initial particles | 9 291 763 |
| No. of final particles | 278 638 |
| Symmetry imposed | C1 |
| Refinement and validation | |
| Initial model used | AF-P38567-F1-v4 (AF2 prediction) |
| Software | CryoSPARC [39] |
| Map resolution (Å) (global) | 3.1 |
| FSC threshold | 0.143 |
| Map sharpening *B* factor ($Å^2$) | 119.5 |
| R.m.s. deviations | |
| Bond lengths (Å) | 0.006 |
| Bond angles (°) | 1.029 |
| Rotamer outliers (%) | 0.28 |
| B factors ($Å^2$) min/max/mean | |
| Protein | 39.63/121.77/63.35 |
| Ligand | 50.49/71.32/59.96 |
| Validation | |
| Clash score | 17.05 |
| MolProbity score | 2.20 |
| Poor rotamers (%) | 0.56 |
| Composition (#) | |
| Non-hydrogen atoms | 6479 |
| Protein residues | 829 |
| Ligand | NAG: 5 |
| Ramachandran plot statistics | |
| Allowed (%) | 7.57 |
| Favored (%) | 92.43 |

of the EGF-like domains, it has been demonstrated that the EGF-like domain containing three disulfide bonds has evolved from those with four disulfide bonds [42]. Plausibly, the atypical EGF-like domain of PH-20 might contribute to its functional role in zona pellucida binding [43].

### 2.4 | The Active Site Groove

The catalytic mechanism of bvHyal has been proposed [35], which closely resembles the substrate-assisted mechanism of chitin degrading enzymes [44]. In this mechanism, three residues—Asp111, Glu113, Tyr227—play critical catalytic roles. These residues are invariant across mammalian hyaluronidases and correspond to Asp146, Glu148, and Tyr264 in PH-20 at spatially equivalent positions, indicating that insect and mammalian hyaluronidases share a conserved catalytic mechanism.

While the overall structure of the central catalytic domain is similar in the three hyaluronidases, they differ from each other in details at regions lining the catalytic groove. Previous study with human HYAL-1 proposed a sequence alignment wherein Asp292 of HYAL-1 corresponds to Asp310 of PH-20 [34]. However, our structure-based alignment shows (Figure S1) that the position is actually occupied by Thr309 in PH-20 (Figure 2C). This particular position is located within the active site groove, forming the binding site for HA, a substrate characterized by its negative charge [35]. The difference in the optimal pH might be due to an involvement Asp292 of HYAL-1 in HA binding, necessitating a pH environment around 3.9 to maintain its side chain in the protonated state, to interact with negatively charged HA. In contrast, this pH-dependent binding constraint could be alleviated in PH-20, because Thr309 occupies the spatially equivalent position. BvHyal, which exhibits a wide pH-activity profile has Gln271 at the spatially equivalent position [45]. Notably, sequence alignment shows that Thr309 of PH-20 is identically conserved in both bovine (Uniprot ID: Q2YDK3) and rat testicular hyaluronidases (Uniprot ID: Q62803) (Figure S1), which exhibit pH optima at pH 4.0 and pH 6.0 [46, 47].

In summary, our structural analyses might serve as a foundation for studying the functional mechanism of PH-20 in the recognition of the zona pellucida layer of egg and the hydrolysis of HA in that particular environment.

## 3 | Materials and Methods

### 3.1 | Cloning, Expression, and Purification of PH-20 and 79C11Fab

Human PH-20 sequences, spanning residues Asn37 to Phe468, were codon-optimized, synthesized by Genscript, and subcloned into the pcDNA3.4-TOPO vector (Invitrogen) with a C-terminal polyhistidine tag. CHO-S cells (Gibco) were transfected with the plasmids (0.8 μg/mL) when the cell density reached $6 \times 10^{10}$ cells/mL. The transfected cells were



Petitioner Merck, Ex. 1126, p. 1069
Merck Sharp & Dohme LLC v. Halozyme Inc.
PGR2025-00003

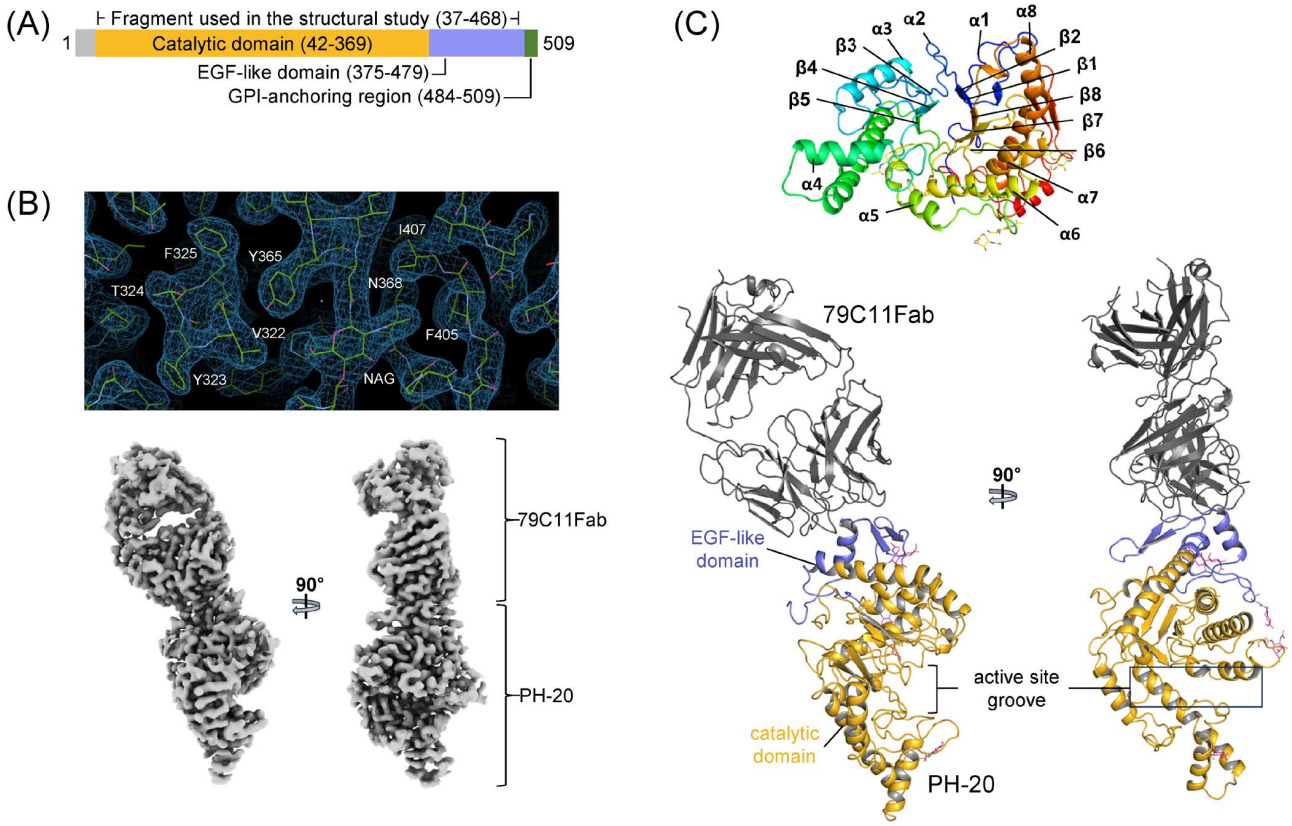


**FIGURE 1** | Cryo-EM structure of PH-20-79C11Fab. (A) Schematic drawing of full-length PH-20 construct. (B) The top panel shows the quality of the final averaged electron density map, highlighting the region around N-glycosylated Asn368. Below, the overall electron density map is displayed in two orientations. (C) The top panel presents a top-down view of the (β/α)8-barrel with labeled β-strands. Below are ribbon diagrams in two orientations, where the catalytic domain of PH-20 is depicted in gold, the EGF-like domain in violet, and 79C11Fab in gray.

incubated for 6 days at 32°C. For harvesting, cells were centrifuged at 10,000 rpm for 30 min to collect the supernatant. The supernatant was first purified using ion exchange chromatography (IEX) with a Q Sepharose column (Cytiva). Specifically, the supernatant was run through the column and washed with five column volumes (CV) of buffer A (20 mM $Na_2HPO_4$, pH 7.5). Buffer B (20 mM $Na_2HPO_4$, pH 7.5, 500 mM NaCl) was then applied to the column with a salt concentration gradient ranging from 0% to 100%. Subsequently, PH-20 purified from IEX was applied to a HisTrap HP column (Cytiva), equilibrated with 20 mM $Na_2HPO_4$ (pH 7.5), 500 mM NaCl, and 35 mM imidazole. To elute the bound PH-20 from the column, 3 CV of the equilibration buffer containing 200 mM imidazole was applied. The elution was dialyzed against 20 mM $Na_2HPO_4$, (pH 7.5) and 100 mM NaCl.

The heavy and light chain genes for 79C11Fab were synthesized (IDT) and sub-cloned into the pCEP4 vectors (Invitrogen). CHO-S cells (Gibco) were co-transfected with the vectors containing subcloned heavy and light chain genes for co-expression and cultured for 7 days. Cells were discarded by centrifugation, and the supernatant medium was filtered through 0.45 μm filters (Millipore). Collected medium was loaded onto Ni-NTA resin (Thermo Scientific) and eluted with 250 mM imidazole in 20 mM Tris–HCl (pH 7.5) and 150 mM NaCl. The eluted fractions were further purified with Superdex 75 column (Cytiva) and concentrated.

### 3.2 | Single-Particle Cryo-EM Analysis

An equimolar mixture of PH-20 and 79C11Fab were incubated on ice for 30 min, and the PH-20-79C11Fab complex was purified by using Superdex 200 column (Cytiva). 3 μL of the complex at 0.1 mg/mL concentration was applied to glow-discharged (at 15 mA for 1 min) and graphene oxide-coated Quantifoil R1.2/1.3 (300 mesh) grid. Using a TFS Vitrobot Mark IV set at 100% humidity and 15°C, the grid was blotted for 3 s with blotting force at −15 and vitrified by plunging into liquid ethane. Data collection was performed with a TFS Krios G4 300 kV microscope equipped with Gatan K3 BioQuantum detector. A total of 20,709 movies were recorded at a nominal magnification of 130,000 at 0.664 Å pixel value with defocus ranging −0.8 to −2.3 μm with total dose of 69 $e^-$/Å and 3.85 s exposure time. To process the acquired data, CryoSPARC v4.2.1 [39] was used. Imported movies were patch motion corrected and patch CTF estimation was performed. After curation of micrographs, 16,845 micrographs were accepted, where criteria such as relative ice thickness (up to 1.3) and CTF fit resolution (up to 9 Å) were used to eliminate low-quality micrographs. From 16,845 micrographs, 9,291,763



Petitioner Merck, Ex. 1126, p. 1070
Merck Sharp & Dohme LLC v. Halozyme Inc.
PGR2025-00003

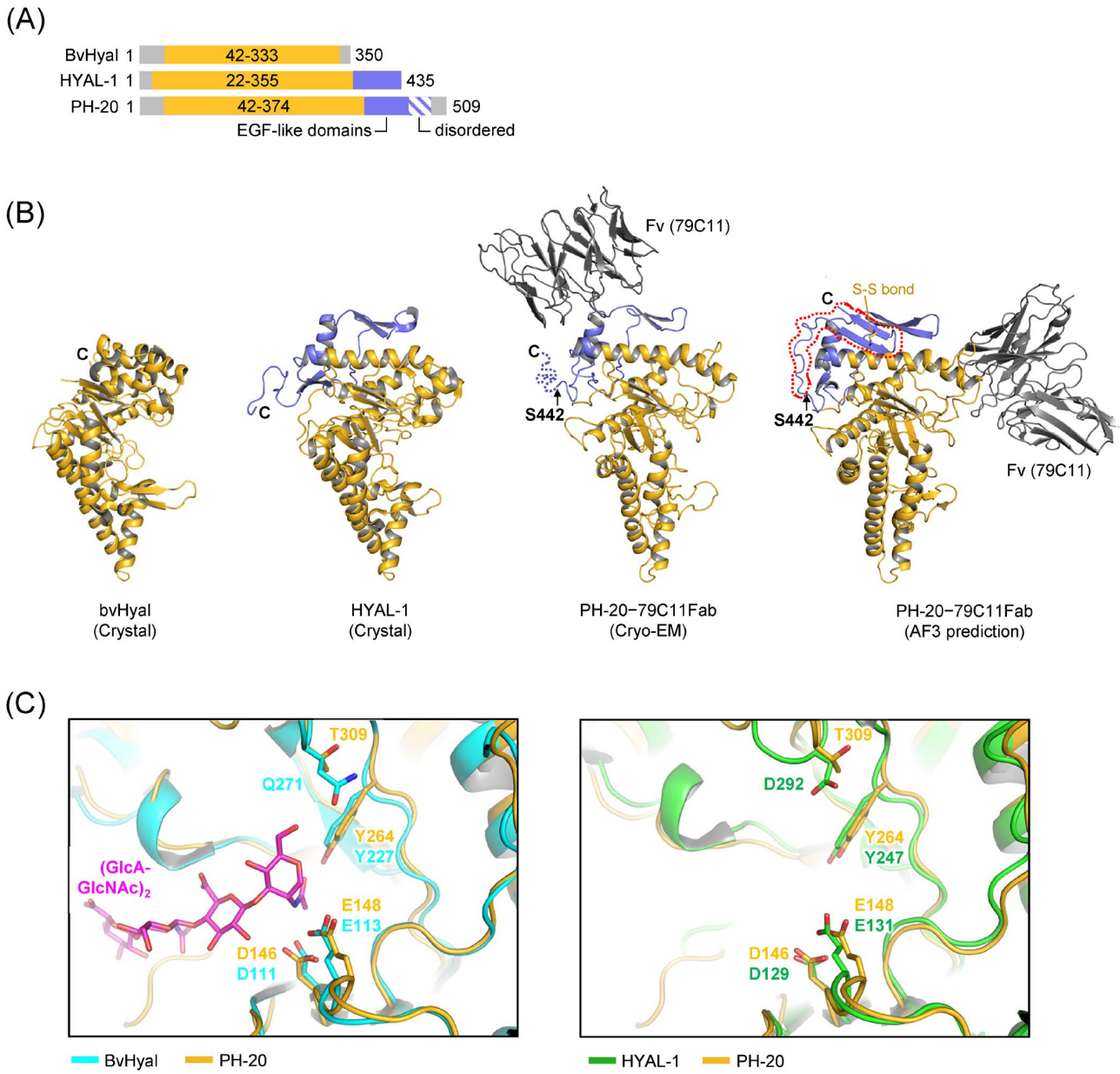


**FIGURE 2** | Structural comparison of hyaluronidases. (A) Schematic drawings of full-length bvHyal, HYAL-1 and PH-20 constructs. Fragments used for each structural study are colored in gold and violet. (B) Displayed in the same orientations are the crystal structure of bvHyal (PDB ID: 1FCV), HAYL-1 (PDB ID: 2PE4), the cryo-EM structure of PH-20-79C11Fv and an AF3-predicted model of PH-20-79C11Fv. The EGF-like domain is shown in violet. Red dotted lines on the predicted model indicate the disordered segment in the EGF-like domain from the experimental structure. The disulfide bond between Cys458 and Cys464 is marked, which is absent in HYAL-1. (C) The structures of PH-20 (gold) and bvHyal (cyan) are superposed. The HA tetramer bound to bvHyal is shown in magenta (Left). The structures of PH-20 (gold) and HYAL-1 (green) are superposed (Right). T309 of PH-20 and Q271 of bvHyal and D292 of HYAL-1 occupying the same spatial position are shown in sticks. The three critical catalytic residues are labeled (D146, E148, Y264). Relative to PH-20, the root-mean-square (RMS) deviations for bvHyal and HYAL-1 are 1.44 Å and 1.65 Å, respectively, for all superposed Cα atoms.

particles were picked with a 200 Å particle diameter, based on templates obtained from previous screen data. Picked particles were inspected and extracted from micrographs with box size of 400 Å and 4X binning factor for further processing. A number of 2D classification were conducted and 670,188 particles were finally extracted at full resolution. The extracted particles were subjected to ab initio 3D reconstruction with 2 classes at initial and maximum resolution of 20 and 8 Å, respectively. Iterative rounds of heterogeneous and homogeneous refinements were conducted to eliminate unwanted particles. Final 278,638 particles were subjected to non-uniform refinement, yielding a map with a resolution of 3.1 Å based on the gold standard Fourier shell correlation with a criterion of 0.143 (Figure S2). The map and a predicted structure of PH-20 by AlphaFold2 [38] were used as a template for model building using Coot [48], and refinement was carried out with real space refinement module in the Phenix [49].



Petitioner Merck, Ex. 1126, p. 1071
Merck Sharp & Dohme LLC v. Halozyme Inc.
PGR2025-00003

## Author Contributions

**Seong-Bin Im:** data curation, writing – original draft, writing – review and editing, conceptualization, investigation, methodology, validation, visualization, formal analysis. **Hyung Nam Song:** investigation, writing – review and editing, validation, conceptualization, data curation, methodology. **Tae-Kyeong Jeong:** investigation, writing – review and editing, validation, methodology, data curation. **Nayun Kim:** investigation, validation, writing – review and editing, methodology. **Kyuwan Kim:** investigation, validation, writing – review and editing, conceptualization. **Soon-Jae Park:** investigation, writing – review and editing, validation, conceptualization, supervision, funding acquisition. **Byung-Ha Oh:** conceptualization, investigation, funding acquisition, writing – original draft, methodology, validation, writing – review and editing, project administration, supervision, formal analysis.


## Acknowledgments

We thank Dr. Ji-Joon Song for his assistance with cryo-EM data collection and processing. This study utilized the cryo-EM microscopes at the Korea Institute for Basic Science and the KAIST Analysis Center for Research Advancement, Republic of Korea. The research was supported by Alteogen Inc. and the National Research Foundation of Korea (Grant Nos. 2023R1A2C3007329, NRF-2021M3A9G8025599, RS-2024-00508861, and RS-2024-00467046).


## Conflicts of Interest

The authors declare no conflicts of interest.

## Data Availability Statement

The coordinates of the structure have been deposited in the Protein Data Bank and in the Electron Microscopy Data Bank with the accession codes 9JUB and EMD-61826 under the condition of immediate release upon publication of the manuscript.

## Peer Review

The peer review history for this article is available at https://www.webofscience.com/api/gateway/wos/peer-review/10.1002/prot.26788.

## References


1. M. J. Jedrzejas and R. Stern, "Structures of Vertebrate Hyaluronidases and Their Unique Enzymatic Mechanism of Hydrolysis," *Proteins* 61 (2005): 227–238, https://doi.org/10.1002/prot.20592.

2. R. Stern and M. J. Jedrzejas, "Hyaluronidases: Their Genomics, Structures, and Mechanisms of Action," *Chemical Reviews* 106 (2006): 818–839, https://doi.org/10.1021/cr050247k.

3. T. C. Laurent and J. R. Fraser, "Hyaluronan," *FASEB Journal: Official Publication of the Federation of American Societies for Experimental Biology* 6, no. 7 (1992): 2397–2404.

4. B. P. Toole, "Hyaluronan: From Extracellular Glue to Pericellular Cue," *Nature Reviews. Cancer* 4 (2004): 528–539, https://doi.org/10.1038/nrc1391.

5. J. R. Fraser, T. C. Laurent, and U. B. Laurent, "Hyaluronan: Its Nature, Distribution, Functions and Turnover," *Journal of Internal Medicine* 242 (1997): 27–33, https://doi.org/10.1046/j.1365-2796.1997.00170.x.

6. M. K. Cowman, T. A. Schmidt, P. Raghavan, and A. Stecco, "Viscoelastic Properties of Hyaluronan in Physiological Conditions," *F1000Res* 4 (2015): 622, https://doi.org/10.12688/f1000research.6885.1.

7. T. C. Laurent, U. B. Laurent, and J. R. Fraser, "The Structure and Function of Hyaluronan: An Overview," *Immunology and Cell Biology* 74 (1996): A1–A7, https://doi.org/10.1038/icb.1996.32.

8. S. Misra, V. C. Hascall, R. R. Markwald, and S. Ghatak, "Interactions Between Hyaluronan and Its Receptors (CD44, RHAMM) Regulate the Activities of Inflammation and Cancer," *Frontiers in Immunology* 6 (2015): 201, https://doi.org/10.3389/fimmu.2015.00201.

9. A. B. Csoka, G. I. Frost, T. Wong, and R. Stern, "Purification and Microsequencing of Hyaluronidase Isozymes From Human Urine," *FEBS Letters* 417 (1997): 307–310, https://doi.org/10.1016/s0014-5793(97)01309-4.

10. A. Aruffo, I. Stamenkovic, M. Melnick, C. B. Underhill, and B. Seed, "CD44 Is the Principal Cell Surface Receptor for Hyaluronate," *Cell* 61 (1990): 1303–1313, https://doi.org/10.1016/0092-8674(90)90694-a.

11. S. Garantziotis and R. C. Savani, "Hyaluronan Biology: A Complex Balancing Act of Structure, Function, Location and Context," *Matrix Biology* 78-79 (2019): 1–10, https://doi.org/10.1016/j.matbio.2019.02.002.

12. X. Tian, J. Azpurua, C. Hine, et al., "High-Molecular-Mass Hyaluronan Mediates the Cancer Resistance of the Naked Mole Rat," *Nature* 499 (2013): 346–349, https://doi.org/10.1038/nature12234.

13. Z. Zhang, X. Tian, J. Y. Lu, et al., "Increased Hyaluronan by Naked Mole-Rat Has2 Improves Healthspan in Mice," *Nature* 621 (2023): 196–205, https://doi.org/10.1038/s41586-023-06463-0.

14. G. I. Frost, A. B. Csoka, T. Wong, and R. Stern, "Purification, Cloning, and Expression of Human Plasma Hyaluronidase," *Biochemical and Biophysical Research Communications* 236 (1997): 10–15, https://doi.org/10.1006/bbrc.1997.6773.

15. A. B. Csoka, S. W. Scherer, and R. Stern, "Expression Analysis of Six Paralogous Human Hyaluronidase Genes Clustered on Chromosomes 3p21 and 7q31," *Genomics* 60 (1999): 356–361, https://doi.org/10.1006/geno.1999.5876.

16. H. Harada and M. Takahashi, "CD44-Dependent Intracellular and Extracellular Catabolism of Hyaluronic Acid by Hyaluronidase-1 and -2," *Journal of Biological Chemistry* 282 (2007): 5597–5607, https://doi.org/10.1074/jbc.M608358200.

17. N. Maeda, M. Palmarini, C. Murgia, and H. Fan, "Direct Transformation of Rodent Fibroblasts by Jaagsiekte Sheep Retrovirus DNA," *Proceedings of the National Academy of Sciences of the United States of America* 98 (2001): 4449–4454, https://doi.org/10.1073/pnas.071547598.

18. S. K. Rai, F. M. Duh, V. Vigdorovich, A. Danilkovitch-Miagkova, M. I. Lerman, and A. D. Miller, "Candidate Tumor Suppressor HYAL2 Is a Glycosylphosphatidylinositol (GPI)-Anchored Cell-Surface Receptor for Jaagsiekte Sheep Retrovirus, the Envelope Protein of Which Mediates Oncogenic Transformation," *Proceedings of the National Academy of Sciences of the United States of America* 98 (2001): 4443–4448, https://doi.org/10.1073/pnas.071572898.

19. R. Hemming, D. C. Martin, E. Slominski, et al., "Mouse Hyal3 Encodes a 45- to 56-kDa Glycoprotein Whose Overexpression Increases Hyaluronidase 1 Activity in Cultured Cells," *Glycobiology* 18 (2008): 280–289, https://doi.org/10.1093/glycob/cwn006.

20. V. Atmuri, D. C. Martin, R. Hemming, et al., "Hyaluronidase 3 (HYAL3) Knockout Mice Do Not Display Evidence of Hyaluronan Accumulation," *Matrix Biology* 27 (2008): 653–660, https://doi.org/10.1016/j.matbio.2008.07.006.

21. T. Kaneiwa, S. Mizumoto, K. Sugahara, and S. Yamada, "Identification of Human Hyaluronidase-4 as a Novel Chondroitin Sulfate Hydrolase That Preferentially Cleaves the Galactosaminidic Linkage in the Trisulfated Tetrasaccharide Sequence," *Glycobiology* 20 (2010): 300–309, https://doi.org/10.1093/glycob/cwp174.

22. L. Bohaumilitzky, A. K. Huber, E. M. Stork, S. Wengert, F. Woelfl, and H. Boehm, "A Trickster in Disguise: Hyaluronan's Ambivalent Roles in the Matrix," *Frontiers in Oncology* 7 (2017): 242, https://doi.org/10.3389/fonc.2017.00242.

23. G. N. Cherr, A. I. Yudin, and J. W. Overstreet, "The Dual Functions of GPI-Anchored PH-20: Hyaluronidase and Intracellular Signaling,"





Petitioner Merck, Ex. 1126, p. 1072
Merck Sharp & Dohme LLC v. Halozyme Inc.
PGR2025-00003

*Matrix Biology* 20 (2001): 515–525, https://doi.org/10.1016/s0945-053x(01)00171-8.

24. E. Kim, D. Baba, M. Kimura, M. Yamashita, S. Kashiwabara, and T. Baba, "Identification of a Hyaluronidase, Hyal5, Involved in Penetration of Mouse Sperm Through Cumulus Mass," *Proceedings of the National Academy of Sciences of the United States of America* 102 (2005): 18028–18033, https://doi.org/10.1073/pnas.0506825102.

25. S. Reitinger, G. T. Laschober, C. Fehrer, B. Greiderer, and G. Lepperdinger, "Mouse Testicular Hyaluronidase-Like Proteins SPAM1 and HYAL5 But Not HYALP1 Degrade Hyaluronan," *Biochemical Journal* 401 (2007): 79–85, https://doi.org/10.1042/BJ20060598.

26. M. A. Printz, S. S. Dychter, E. P. DeNoia, et al., "A Phase I Study to Evaluate the Safety, Tolerability, Pharmacokinetics, and Pharmacodynamics of Recombinant Human Hyaluronidase PH20 Administered Intravenously in Healthy Volunteers," *Current Therapeutic Research, Clinical and Experimental* 93 (2020): 100604, https://doi.org/10.1016/j.curtheres.2020.100604.

27. D. S. C. Sharma and M. A. Lahiri, "Use of Hyaluronidase in Plastic Surgery: A Review," *Journal of Plastic, Reconstructive & Aesthetic Surgery* 74 (2021): 1610–1614, https://doi.org/10.1016/j.bjps.2021.03.125.

28. G. C. Weber, B. A. Buhren, H. Schrumpf, J. Wohlrab, and P. A. Gerber, "Clinical Applications of Hyaluronidase," *Advances in Experimental Medicine and Biology* 1148 (2019): 255–277, https://doi.org/10.1007/978-981-13-7709-9_12.

29. K. W. Locke, D. C. Maneval, and M. J. LaBarre, "ENHANZE Drug Delivery Technology: A Novel Approach to Subcutaneous Administration Using Recombinant Human Hyaluronidase PH20," *Drug Delivery* 26 (2019): 98–106, https://doi.org/10.1080/10717544.2018.1551442.

30. R. L. Wasserman, I. Melamed, M. R. Stein, et al., "Recombinant Human Hyaluronidase-Facilitated Subcutaneous Infusion of Human Immunoglobulins for Primary Immunodeficiency," *Journal of Allergy and Clinical Immunology* 130 (2012): e911, https://doi.org/10.1016/j.jaci.2012.06.021.

31. H. Jung, "Hyaluronidase: An Overview of Its Properties, Applications, and Side Effects," *Archives of Plastic Surgery* 47 (2020): 297–300, https://doi.org/10.5999/aps.2020.00752.

32. G. J. Doherty, M. Tempero, and P. G. Corrie, "HALO-109-301: A Phase III Trial of PEGPH20 (With Gemcitabine and Nab-Paclitaxel) in Hyaluronic Acid-High Stage IV Pancreatic Cancer," *Future Oncology* 14 (2018): 13–22, https://doi.org/10.2217/fon-2017-0338.

33. L. Morosi, M. Meroni, P. Ubezio, et al., "PEGylated Recombinant Human Hyaluronidase (PEGPH20) Pre-Treatment Improves Intra-Tumour Distribution and Efficacy of Paclitaxel in Preclinical Models," *Journal of Experimental & Clinical Cancer Research* 40 (2021): 286, https://doi.org/10.1186/s13046-021-02070-x.

34. K. L. Chao, L. Muthukumar, and O. Herzberg, "Structure of Human Hyaluronidase-1, a Hyaluronan Hydrolyzing Enzyme Involved in Tumor Growth and Angiogenesis," *Biochemistry* 46 (2007): 6911–6920, https://doi.org/10.1021/bi700382g.

35. Z. Markovic-Housley, G. Miglierini, L. Soldatova, P. J. Rizkallah, U. Muller, and T. Schirmer, "Crystal Structure of Hyaluronidase, a Major Allergen of Bee Venom," *Structure* 8 (2000): 1025–1035, https://doi.org/10.1016/s0969-2126(00)00511-6.

36. B. Pang, J. He, W. Zhang, et al., "Active Expression of Human Hyaluronidase PH20 and Characterization of Its Hydrolysis Pattern," *Frontiers in Bioengineering and Biotechnology* 10 (2022): 885888, https://doi.org/10.3389/fbioe.2022.885888.

37. C. UniProt, "UniProt: The Universal Protein Knowledgebase in 2023," *Nucleic Acids Research* 51 (2023): D523–D531, https://doi.org/10.1093/nar/gkac1052.

38. J. Jumper, R. Evans, A. Pritzel, et al., "Highly Accurate Protein Structure Prediction With AlphaFold," *Nature* 596 (2021): 583–589, https://doi.org/10.1038/s41586-021-03819-2.

39. A. Punjani, J. L. Rubinstein, D. J. Fleet, and M. A. Brubaker, "cryoSPARC: Algorithms for Rapid Unsupervised Cryo-EM Structure Determination," *Nature Methods* 14 (2017): 290–296, https://doi.org/10.1038/nmeth.4169.

40. R. Jansen and M. Gerstein, "Analysis of the Yeast Transcriptome With Structural and Functional Categories: Characterizing Highly Expressed Proteins," *Nucleic Acids Research* 28 (2000): 1481–1488, https://doi.org/10.1093/nar/28.6.1481.

41. J. Abramson, J. Adler, J. Dunger, et al., "Accurate Structure Prediction of Biomolecular Interactions With AlphaFold 3," *Nature* 630 (2024): 493–500, https://doi.org/10.1038/s41586-024-07487-w.

42. M. A. Wouters, I. Rigoutsos, C. K. Chu, L. L. Feng, D. B. Sparrow, and S. L. Dunwoodie, "Evolution of Distinct EGF Domains With Specific Functions," *Protein Science* 14 (2005): 1091–1103, https://doi.org/10.1110/ps.041207005.

43. G. R. Hunnicutt, P. Primakoff, and D. G. Myles, "Sperm Surface Protein PH-20 Is Bifunctional: One Activity Is a Hyaluronidase and a Second, Distinct Activity Is Required in Secondary Sperm-Zona Binding," *Biology of Reproduction* 55 (1996): 80–86, https://doi.org/10.1095/biolreprod55.1.80.

44. A. C. T. V. S. Ivo Tews, A. Perrakis, K. S. Wilson, and B. W. Dijkstra, "Substrate-Assisted Catalysis Unifies Two Families of Chitinolytic Enzymes," *Journal of the American Chemical Society* 119, no. 34 (1997): 7954–7959.

45. A. Ilias, K. Liliom, B. Greiderer-Kleinlercher, S. Reitinger, and G. Lepperdinger, "Unbinding of Hyaluronan Accelerates the Enzymatic Activity of Bee Hyaluronidase," *Journal of Biological Chemistry* 286 (2011): 35699–35707, https://doi.org/10.1074/jbc.M111.263731.

46. E. S. Hofinger, G. Bernhardt, and A. Buschauer, "Kinetics of Hyal-1 and PH-20 Hyaluronidases: Comparison of Minimal Substrates and Analysis of the Transglycosylation Reaction," *Glycobiology* 17 (2007): 963–971, https://doi.org/10.1093/glycob/cwm070.

47. G. J. Seaton, L. Hall, and R. Jones, "Rat Sperm 2B1 Glycoprotein (PH20) Contains a C-Terminal Sequence Motif for Attachment of a Glycosyl Phosphatidylinositol Anchor. Effects of Endoproteolytic Cleavage on Hyaluronidase Activity," *Biology of Reproduction* 62 (2000): 1667–1676, https://doi.org/10.1095/biolreprod62.6.1667.

48. P. Emsley, B. Lohkamp, W. G. Scott, and K. Cowtan, "Features and Development of Coot," *Acta Crystallographica. Section D, Biological Crystallography* 66 (2010): 486–501, https://doi.org/10.1107/S0907444910007493.

49. P. D. Adams, P. V. Afonine, G. Bunkoczi, et al., "PHENIX: A Comprehensive Python-Based System for Macromolecular Structure Solution," *Acta Crystallographica. Section D, Biological Crystallography* 66 (2010): 213–221, https://doi.org/10.1107/S0907444909052925.

**Supporting Information**

Additional supporting information can be found online in the Supporting Information section.



Petitioner Merck, Ex. 1126, p. 1073
Merck Sharp & Dohme LLC v. Halozyme Inc.
PGR2025-00003